Coastal Engineering 88 (2014) 123–130

Contents lists available at ScienceDirect

Coastal Engineering

journal homepage: www.elsevier.com/locate/coastaleng

# Flow convergence at the tip and edges of a viscous swash front — Experimental and analytical modeling

T.E. Baldock *, R. Grayson, B. Torr, H.E. Power

*School of Civil Engineering, University of Queensland, Brisbane, Queensland 4072, Australia*

ARTICLE INFO

*Article history:*
Received 6 November 2013
Received in revised form 23 February 2014
Accepted 26 February 2014
Available online xxxx

*Keywords:*
Swash
Wave tip
Viscous flow
Shear stress
Friction
Flow convergence

ABSTRACT

The details of flow at the tip of a viscous swash front are important to describe the propagation of the wave, the bed shear and to estimate material transport rates and impact forces. This paper presents novel experimental data illustrating the convergence of fluid at swash fronts generated by dam-break flows. Very viscous fluids (detergents) were used to slow the flow sufficiently to enable video tracking of particles on the free surface and within the interior of the flow. The experiments were performed both up a slope and on a horizontal bed. The particle tracking shows that surface particles travel faster than the mean flow, converge on the swash tip and then rapidly decelerate, a process that will induce a high bed shear stress at the swash tip as observed in recent experiments. Particles also converge on the wall boundaries because of the no-slip condition. A simple analytical model is developed to estimate the ratio of the velocity of surface particles and the wave front. For laminar flows, this ratio is found to be 3/2, independent of the bed slope and flow depth, and is in good agreement with the experimental data. The same model approach suggests a ratio of 8/7 for turbulent flows. This flow convergence does not appear to be included in either analytical modeling of the tip region or in basal resistance laws for the swash front and would modify the momentum equation at the swash tip [c.f. Hogg and Pritchard, 2004] and the kinematic boundary condition at the shoreline. The flow convergence is consistent with observations of the behavior and build-up of buoyant debris at the leading edge of tsunami wave front and can be observed in natural swash flows on beaches.



## 1. Introduction

More accurate descriptions of the flow details at the tip of a swash front are of relevance for improving models for the propagation of waves on beaches and in dam-break flows, for determining the basal resistance in the tip region, and for estimating sediment transport rates and impact forces (Emmett and Moodie, 2008; Hogg and Pritchard, 2004; Othman et al., 2014; Yeh, 2006). Current models, based around the application of an empirical semi-analytical force balance (Hughes, 1995; Puleo and Holland, 2001) or the non-linear shallow water equations assume that the wave-tip region propagates as a solid tip with a uniform flow in the region immediately behind the tip (Chanson, 2006; Whitham, 1955). This assumption also leads to the assumption that the kinematic condition at the wave tip (shoreline) is that fluid particles at the shoreline stay at the shoreline, or equivalently that the velocity of the shoreline and fluid velocity are equal at the shoreline (e.g., Brocchini et al., 2002), which is the most widely adopted shoreline boundary condition for coastal numerical models. The effects of resistance are modeled with a friction coefficient that is applied to the interface between the wave and the bed. The effect of this simplification is that the surface particles propagate at the celerity of the swash tip, as does the momentum. In practice, there is shear in the velocity profile and a boundary layer occurs at the front (Ancey et al., 2009, 2012; Andreini et al., 2012; Hogg and Pritchard, 2004).

Both swash and dam-break wave fronts are one class of a wide range of shallow water flows which are influenced by friction, see Chanson (2006) for a comprehensive review. However, direct measurements of the shear stress at the tip of swash wave fronts do not show good agreement with conventional friction coefficients (Barnes and Baldock, 2010; O'Donoghue et al., 2010); the shear stress within the tip region is particularly high and then decreases very rapidly away from the front. Barnes and Baldock (2010) suggested that this might be because the no-slip condition at the bed leads to flow convergence at the swash tip, which is then overrun by the fluid behind. This mechanism will lead to the constant injection of high momentum fluid into the boundary layer at the swash tip, potentially generating high bed shear stresses.

Prior studies have shown that dam-break velocities increase non-linearly away from the bed (e.g., Ancey et al., 2009, 2012; Andreini et al., 2012; Hogg and Pritchard, 2004). Here we show that this vertical flow structure in a dam break leads to convergence near the leading tip. While a non-uniform velocity profile does not necessarily ensure flow convergence, with hindsight, flow convergence can be readily inferred

* Corresponding author at: School of Civil Engineering, University of Queensland, Brisbanem QLD, 4072.

http://dx.doi.org/10.1016/j.coastaleng.2014.02.008
0378-3839/

from such prior observations. However, we are unaware of previous experiments that present observations of such flow convergence, or a simple theory to determine the rate of convergence.

This paper considers this issue and presents new experiments that aim to illustrate the details of the flow at the tip of a viscous wave front induced by dam-break swash flows. Inspired by observations of the creeping and rolling motion of lava flows (see e.g., Griffiths, 2000), very viscous fluids (detergents) are used to slow the flow sufficiently to enable video tracking of particles on the free surface and within the interior of the flow. An analytical description of rate of flow convergence at the wave front is developed, and is compared to the measured data, with good agreement. This provides a basis for extrapolation to turbulent flows in water. The paper is organized as follows. Section 2 outlines a new theoretical analysis to predict the rate of flow convergence toward the tip, which is found to be consistent with the viscous flow solution of Huppert (1982). Section 3 presents the details of the experimental setup and particle tracking technique. Results, including photographs and particle trajectories are summarized in Section 4. Final conclusions follow in Section 5.

## 2. Theory

The present work is concerned with the flow on the free surface of the fluid and in the interior of the flow, rather than the details at the contact line. Consequently, it is not necessary to consider the contact line dynamics for an overall description, consistent with the approach of Huppert (1982). The key assumption is that there is a quasi-steady self-similar flow condition at the swash front, defined in Fig. 1. With this assumption, from continuity, and with discharge per unit width q(x), the tip celerity, $c$, will be equal to the *mean* flow velocity behind the front, $\overline{u}$:

$$q(x) = \int_0^h u dy = ch = \overline{u}h. \tag{1}$$

Viscous basal drag will result in a non-uniform velocity profile. Taking zero shear stress on the free surface yields a parabolic velocity profile for a laminar flow of fluid with density $\rho$, and dynamic viscosity, $\mu$:

$$u(y) = \frac{1}{2\mu}\rho g \sin\alpha\left(h^2 - y^2\right) \tag{2}$$

with $y$ measured downward and perpendicular to the free surface. Substitution into Eq. (1) gives the mean velocity

$$\overline{u} = \frac{\rho g \sin\alpha h^2}{3\mu} = c. \tag{3}$$

The velocity of surface particles is obtained from Eq. (2) with $y = 0$. Taking the ratio of the velocity of the surface particles, $U_s$, to the mean flow velocity or the tip celerity gives:

$$\frac{U_s}{c} = \frac{U_s}{\overline{u}} = \frac{3}{2} \tag{4}$$

which is independent of the bed slope and the flow depth and is a well-known result for uniform free surface laminar flows. The surface curvature can be accounted for by including a correction term of $-\cot\alpha\, \partial h / \partial x$ in Eq. (2), e.g., Ancey et al., 2012; Hogg and Matson, 2009.

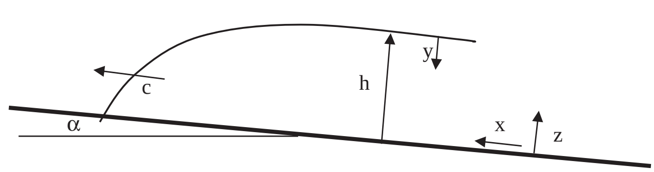


**Fig. 1.** Definition sketch and the coordinate system for a wave front progressing up slope.

However, on integration, the same term occurs in Eq. (3) and therefore cancels in Eq. (4), giving no change in the rate of convergence. It should be noted that very close to the intersection of the wave tip and the bed the assumption of a shallow flow with negligible vertical component becomes invalid, and the horizontal velocity will reduce compared to the theoretical laminar solution. This can be observed in the data of Andreini et al. (2012). A power law can be used as an alternative (approximation) for parabolic or logarithmic boundary layer profile, which simplifies the algebra in the latter case. Taking $z$ measured perpendicular upward from the bed,

$$\frac{u}{U_s} = \left(\frac{z}{h}\right)^{1/n} \tag{5}$$

yielding

$$\overline{u} = U_s \frac{n}{n+1} \tag{6}$$

and hence

$$U_s = c\frac{n+1}{n}. \tag{7}$$

For $n = 2$, $U_s = 3/2c$, corresponding to laminar flows, and for $n = 7$, $U_s = 8/7c$, corresponding to higher Reynolds number turbulent flows (e.g., Daugherty, 1977). Therefore, while it is well known that surface particles travel faster than the mean flow in steady flows, it is the application of this principle at the swash tip that is relevant here, and which yields a near constant relative velocity between the surface particle and the swash tip, the magnitude of which is controlled by the shear in the velocity profile. Clearly, the relative velocity between the fluid particles and swash tip then depends on the elevation of the fluid within the boundary layer. Basal fluid is left behind the wave front, whereas fluid near the surface converges on the wave front. As a uniform velocity profile is approached, the surface velocity approaches the mean velocity (and the tip celerity), which is the conventional model assumption for the leading edge of swash (Hogg and Pritchard, 2004) and dam-break flows (e.g., Chanson, 2006; Whitham, 1955).

Huppert (1982) provided a laminar solution for the far field swash tip position for the problem of a viscous wave front, in that instance propagating downslope:

$$x_{tip} = Dt^{1/3}, \quad D = \left(\frac{9A^2 g \sin\alpha}{4\upsilon}\right)^{1/3} \tag{8}$$

where $A$ is the initial cross-sectional area of the flow and $\nu$ is the kinematic viscosity. The swash tip speed can be derived as:

$$\frac{dx_{tip}}{dt} = \frac{1}{3}Dt^{-2/3}. \tag{9}$$

Huppert (1982) also provides an expression for the depth just behind the swash tip, but not for the surface velocity or the flow profile:

$$h_{tip} = \frac{1.5A}{x_{tip}}. \tag{10}$$

However, Huppert's governing equation is the exact laminar form of the Navier–Stokes equation, so it is assumed here that the surface velocity in that solution is again given by Eq. (2). Combining Eqs. (2), (8), (9) and (10) gives $U_s/c = 3/2$, as before, and independent of slope. Thus, the solutions are consistent and Eqs. (4) and (7) are expected to hold regardless of slope and viscosity. Ancey et al. (2009) provide a more detailed solution for the position of the wave tip and flow depths, including the shape of the surface in the swash tip, which tends quickly to a self-similar shape. Thus the approximation of a quasi-steady self-similar wave front (Fig. 1) in a moving reference frame appears justified. Note that the boundary layer profile may differ from that assumed in Eq. (2) or Eq. (5), e.g., for wave fronts propagating over mobile sediment beds, or very close to the wave front (Ancey et al., 2012), changing the value in Eq. (4) or Eq. (7), but the principle remains the same.

For a non-uniform velocity profile, the true momentum flux is similarly greater than that based on the mean flow velocity. Therefore, for a steady tip velocity, $c = \overline{u}$, an excess flux of momentum enters the tip region compared to that based on the mean flow rate. This excess is given by the usual momentum correction coefficient for shallow water flows (e.g., Hogg and Pritchard, 2004).

$$\beta = \frac{1}{h\overline{u}^2}. \tag{11}$$

For a parabolic laminar flow profile given by Eq. (2), $\beta = 6/5$, and for a power law profile given by Eq. (5), $\beta = \frac{(n+1)^2}{n(n+2)}$. For a turbulent 1/7 power law, $\beta = 1.015$. In both cases, the momentum is advected faster than the mean flow, leading to the injection of fluid with a higher momentum toward the fluid tip and toward the bed boundary (Barnes and Baldock, 2010), providing a mechanism for the relatively high sheer stresses observed at the leading edge of swash flows (Barnes et al., 2009; O'Donoghue et al., 2010).

## 3. Experiments

### 3.1. Apparatus

To study the flow convergence at the swash tip, experiments were performed in a dam-break flume that measured 0.4 m deep, 0.4 m wide and 3.0 m long (Fig. 2), with glass sides and a PVC bed. A lever operated gate, positioned normal to the bed, divided the flume into a 1.01 m long reservoir and a 2 m long 'dry' flat bed. To obtain the desired gradient, $\alpha$, of the flume, the whole flume pivots about the downstream end, and a pulley system was used to raise and lower the flume. A pivoting handle was attached to the gate, and this enables the gate to open to a height of 0.2 m in about 0.15 s, which provides near instantaneous release conditions. The edges and base of the gate were lined with a silicon seal built in-situ around the gate. Together with the addition of some silicon grease, this ensured an excellent near watertight seal without any protruding elements in the flow. Experiments could therefore be performed with "dry" (zero fluid depth) bed conditions downstream from the gate. Two digital video cameras (Panasonic NV-GS300; Canon IXUS 801S; 720 by 576 pixels) were used to capture the propagation of the viscous swash tip and tracer particles. The cameras sampled at 25 and 30 Hz and were mounted looking side-on to the flume (with overlapping field of view if necessary) and looking top-down and front on, with both focused on the swash tip and the region immediately behind the tip. PIV was not adopted due to the requirement to track surface particles, the lack of transparency of the Newtonian fluid, and the need to track the same particle over distances of order 1–2 m.

Two types of detergent were used in the experiments, one detergent being transparent to enable tracking of particles within the interior of the fluid. Table 1 provides a summary of the fluid properties of the detergents used with reference to the material safety data sheets. The densities of the detergents are of the same order as water and their surface tension is lower. Therefore, the primary difference in the fluid properties compared to water is viscosity, as intended. The majority of the experiments were performed with the (green) lower viscosity detergent, which is a Newtonian fluid. Unfortunately, a clear detergent with similar properties could not be obtained in bulk in the required quantities. Selected experiments were performed with the clear detergent to track particles within the body of the flow and at the flume bed. However, given the much higher viscosity of this detergent, the same tests could not be reliably repeated using both detergents, so we cannot compare identical paths of surface particles and interior particles for the same tests. This detergent also exhibited non-Newtonian behavior at higher shear rates, however, it is not anticipated that this significantly alters the conclusions drawn from the data. Temperature variations within the fluids during the experiments were less than 4 °C.

### 3.2. Experimental procedure

The flume was set to the desired angle of tilt and the reservoir was filled to the required level, with the depth of fluid in the reservoir at the gate ($d_o$) measured perpendicular to the bed. Most tests were performed with an upward tilt, to further slow the propagation speed of the tip. This also avoided overtopping of the detergent at the end of the flume and the need to collect and recycle the detergent back into the flume, which introduces dirt and bubbles. A range of different particles were used for flow tracking, from small light Styrofoam balls for surface flows to near neutrally buoyant plastic beads for internal flows and the basal regions. Particle diameters ranged from 3 to 8 mm. Given the densities of the clear detergent and appropriate plastics, in combination with the high viscosity, particles could be suspended at the mid-depth of the reservoir for sufficient time to perform the experiment and with sufficient transparency for video tracking. Similarly, near neutrally buoyant particles were placed downstream of the gate to track flow in the basal region after the initial particle location was overrun by the swash tip. Typically, particles were spaced 25–50 mm apart, on the fluid surface along the flume center line, and on the reservoir side of the gate. The initial spacing of the surface particles could be set accurately by ruler; the spacing of the subsurface particles was less uniform since they move slightly after the initial placement. A sketch of the typical initial position of the particles is provided in Fig. 3. Light

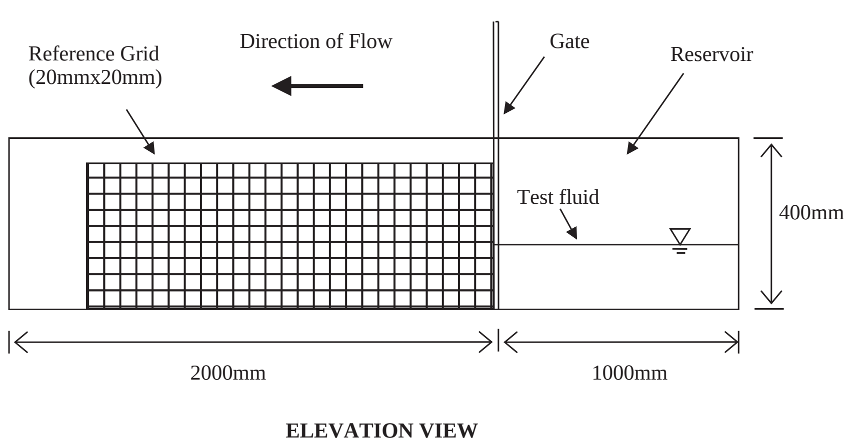


**Fig. 2.** Schematic of dam-break flume.

**Table 1**
Fluid properties.

| Detergent | Detergent 1 | Detergent 2 |
|---|---|---|
| Density (kg/m$^3$) | 1020–1040 | 935 |
| Surface tension (mN/m) | 34 | 18 |
| Viscosity (Pa·s) | 0.8–0.9 | ≈4–5 |
| Color/transparency | Green | Clear |

particles were also placed on the fluid surface within the reservoir, in lines across the flume and in lines parallel to the side walls. The tracks of these particles were used to investigate the influence of the side wall boundary layer. Before running each test, the region downstream of the gate was cleaned of excess fluid; any small seepage just downstream of the gate was wiped out immediately before the gate was opened. Each test therefore corresponds to a swash tip propagating over an initially dry bed (zero fluid depth). Multiple re-runs were performed if high quality video records were not obtained and a number of repeatability tests were conducted to check the consistency of the results.

### 3.3. Data and video analyses

Manual selection was performed to identify the center of each particle and was adopted over automated tracking because of complications induced by the recirculation region, which need to be excluded, and for the purposes of this study, was the simplest approach. Reference coordinates for image processing were set at fixed points on the flume. The particle diameters varied from 3 mm–8 mm. It is estimated that the center of the particle could be identified to an accuracy within 2 mm.

The particle and swash tip displacements are measured parallel to the bed surface and time is measured from the instant of the initial gate opening. Instantaneous particle velocities were determined using the change in displacement between each time step, with averaging over 5 frames. Data is non-dimensionalized as follows (e.g., Chanson, 2006):

$$t = t*\sqrt{\frac{g}{d_o}}, x = \frac{x*}{d_o} \tag{12}$$

where the dimensional variables are starred.

## 4. Results

To illustrate the convergence of the flow on the swash tip, a sequence of three still images extracted from the video is shown in Fig. 4a–c. In Fig. 4a, five particles are visible on the fluid surface behind the swash tip, and this reduces to four and three particles visible behind the swash tip in Fig. 4b and c, respectively, as the swash tip progresses forward. The “missing” particles have converged on the tip and tend to remain there if sufficiently buoyant. Denser but still buoyant particles circulate via the basal layer before rising to the surface, forming a recirculation eddy. The recirculation is not directly relevant to the convergence rate investigated here, but is perhaps indicative of the motion of buoyant debris in such flows. The swash tip progressed forward with a “rolling” motion at the surface, in conjunction with a no-slip condition at the bed. Dussan and Davis (1974) described this “rolling” motion at the front of a single viscous drop, although their focus was the contact line dynamics. Data showing this convergence of the surface particles on the swash tip was initially presented by Baldock et al. (2010), but the theory in Section 2 was lacking at that time. Park et al. (2012) likewise discuss a rolling motion at the contact line during wave reflection on a vertical wall and show that particles are pulled into the wall as the contact line progresses. Goodwin and Homsy (1991) similarly noted that a recirculation field will occur at a wave front when viewed in a reference frame moving with the wave tip.

Displacement time-histories of the swash tip (black line) and five particles are illustrated in Fig. 5. The first three of the five tracked particles are observed to progressively approach the swash tip. Note that both the swash tip and the particles are slowing over time since the wave was progressing upslope in this case. The third particle does not quite reach the tip before flow reversal occurs at the surface. Particles 4 and 5 initially converge on the swash tip, but the rate of convergence slows as the time of flow reversal approaches. Hence, full convergence only occurs over a finite distance behind the tip for a wave propagating up-slope. Fig. 6 shows the displacement of the same particles relative to the swash tip. Initially, the rate of convergence on the swash tip is similar for all particles close to the swash tip; again, those further behind converge more slowly for a wave propagating up slope. At $t \approx 10$ the leading tracked particle reaches the swash tip, and then decelerates very rapidly; similarly for particle 2 at $t \approx 20$. Particle 3 reaches the swash tip at approximately the time of flow reversal when the forward velocity is nearly zero. The rapid deceleration of the fluid particles due to the no slip condition at the bed imparts momentum transfer to the

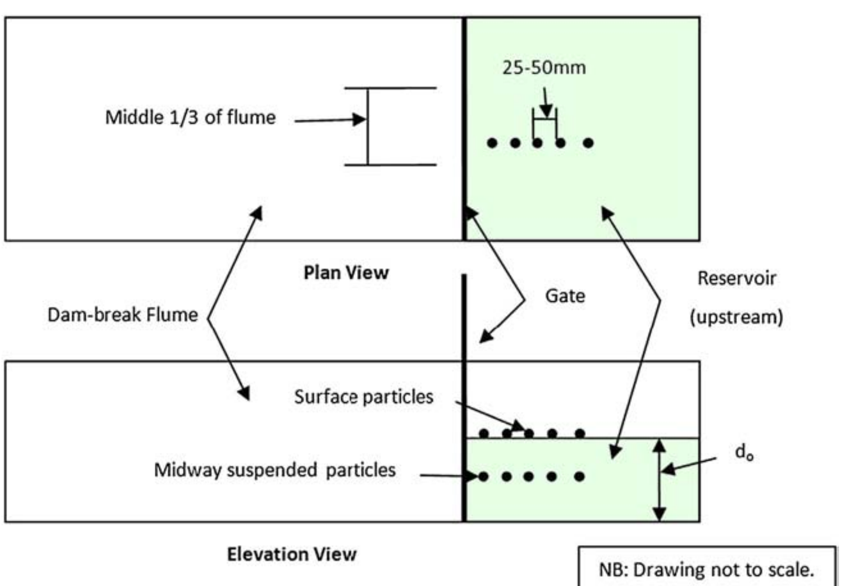


**Fig. 3.** Illustration of initial positions of particles for video tracking. Surface particles were also placed in three lines parallel to the flume walls to investigate boundary wall effects.

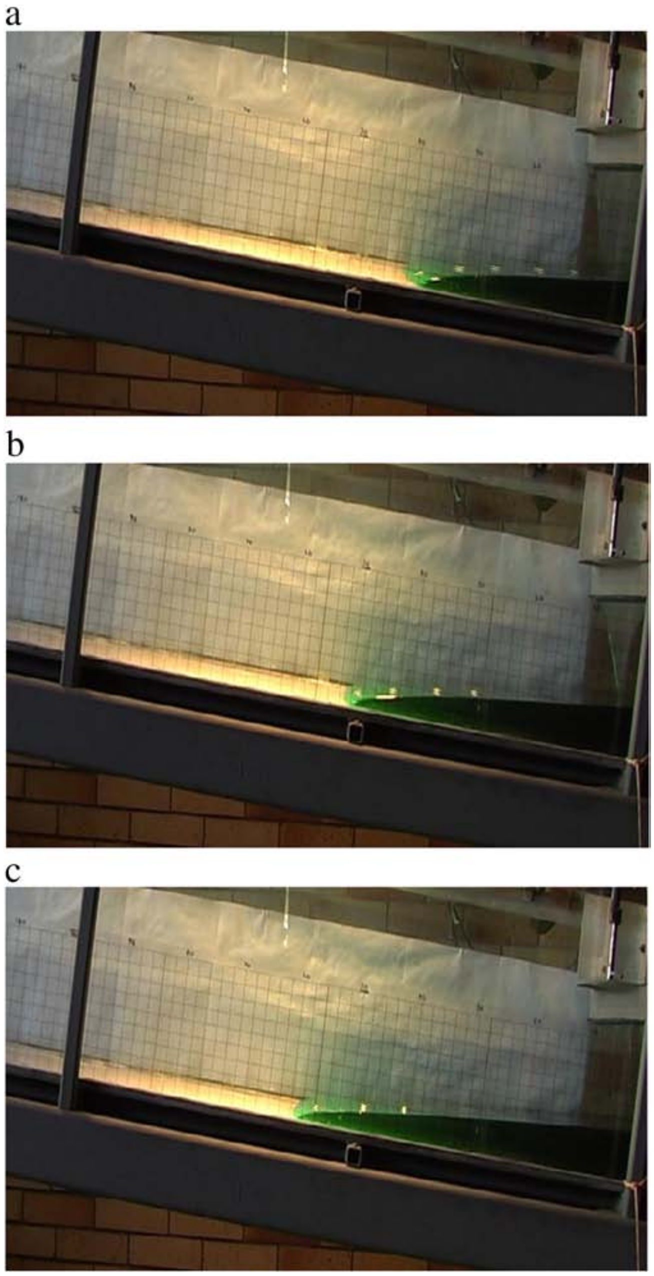

**Fig. 4.** Snapshots of surface particles behind the dam-break tip progressing up a 1:10 slope. $d_o = 0.09$ m.

bed, and is therefore likely to generate a strong localized bed shear stress, as proposed by Barnes and Baldock (2010). A supplementary video of the initial stages of this test is available with the online version of the paper.

For this experiment on an upward sloping bed, the particles that reach the tip of the wave initially converged on the tip at a relatively constant rate (Fig. 6). However, the rate of convergence slowed as the time of flow reversal approaches. This is because the fluid behind the tip reverses flow direction prior to the reversal of motion at the swash tip. This slowing of the rate of convergence does not occur on a horizontal or downward sloping bed. The convergence of the flow on the tip region appears due to the no-slip condition retarding the fluid at the wet–dry interface, which is then overrun by the fluid above and behind the tip region (Barnes and Baldock, 2010). Clearly, near surface sediment will also be advected toward the wave tip. Similarly, buoyant

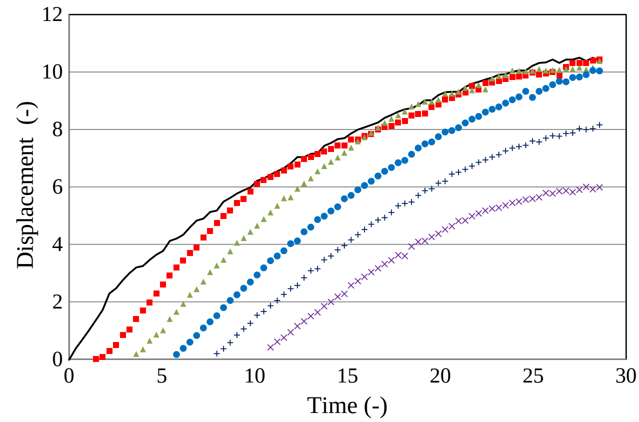


**Fig. 5.** Displacement time-history for five surface particles behind the swash tip. $\alpha = 0.05$, $d_o = 0.12$ m. Detergent 1.

debris close to a wave tip boundary region will also converge on the tip, leading to a build-up of debris at the wave front. Indeed, this convergence of debris toward the wave front can clearly be seen from video footage taken during the Japanese 2012 tsunami at Sendai, see http://youtu.be/J2hUwFo6Vpc. For typical swash flows on beaches, foam patches can be seen to similarly converge on the run-up tip, albeit at a relatively slow rate, consistent with Eq. (7). Further work is required to determine if a parameter exists to define the extent of the convergence zone on upward sloping beaches. If so, such a parameter is likely to depend on the swash boundary conditions, which determine the time of flow reversal (Guard and Baldock, 2007; Pritchard et al., 2008). The rate of convergence is also likely to be higher on highly permeable beaches as a result of loss of fluid at the wave tip.

Consistent with the analysis in Section 2, only particles at elevations where $u$ exceeds $\overline{u}$ converged on the swash tip; particles at locations where $u \approx \overline{u}$ held station relative to the swash tip and particles at locations where $u < \overline{u}$ were left behind. The latter are clearly the particles in the basal region. This is illustrated in Figs. 7 and 8, which show the relative displacement of particles in the upper and central parts of the fluid and those at the bed, respectively. The particles suspended at mid-depth in the flow maintain the same position relative to the swash tip, while the basal particles are left behind, clearly at a rate approximately equal to the tip celerity. Fig. 9 shows the ratio of the surface velocity (estimated from the particle tracking), $\frac{U_s}{c}$ for the three leading particles illustrated in Fig. 5. While there is some noise in the estimate, clearly the data are in very good agreement on average with the estimate of $\frac{U_s}{c} = \frac{3}{2}$

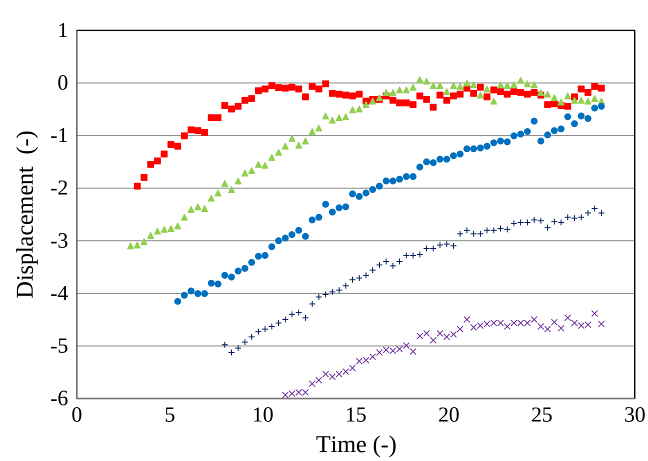


**Fig. 6.** Relative displacement of the swash tip and surface particles in Fig. 5. $\alpha = 0.05$, $d_o = 0.12$ m. Detergent 1.

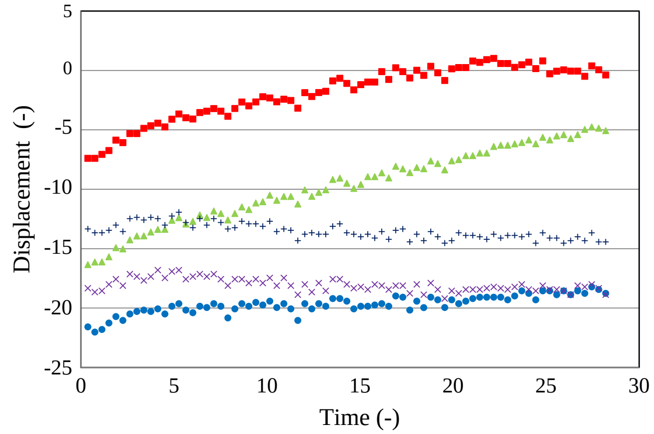


**Fig. 7.** Relative displacement of the swash tip and surface particles (square, triangle) and three particles at mid-depth (dot, plus, cross). $\alpha = 0.033$, $d_o = 0.16$ m. Detergent 2.

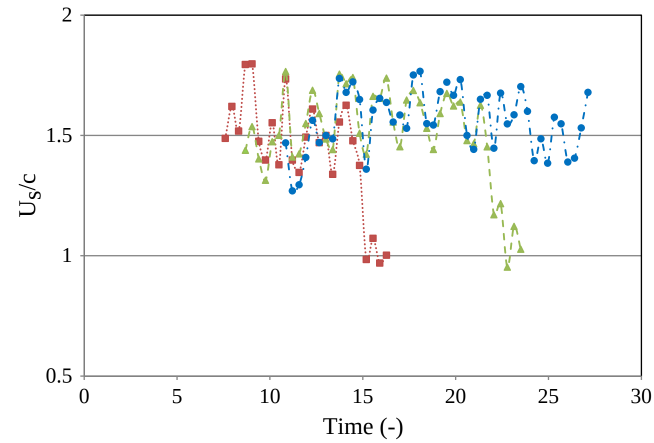


**Fig. 9.** Ratio of the velocity of surface particles to the swash tip celerity, $U_s/c$, for particles 1–3 in Fig. 5. $\alpha = 0.05$, $d_o = 0.12$ m. Detergent 1.

from Section 2. Note that this ratio drops to a value of 1 once the particles reach the swash tip and are trapped in a recirculating eddy. Although the flow is slowing as flow reversal approaches, the mean value of the ratio $\frac{U_s}{c}$ remains remarkably constant until this occurs. Similar particle trajectories and a similar rate of convergence were observed in other tests.

A similar pattern of convergence was observed to occur along the side-wall boundaries. In this region the no-slip condition retards the fluid in the wall boundary layer and the adjacent interior fluid again overruns the wall layer at the wet–dry interface. Fluid particles therefore also converge on the side walls from the center part of the flow. This is illustrated in Figs. 10 and 11, which show snapshots taken from the downstream end of the flume, looking back toward the reservoir, and demonstrate the effects of the wet–dry wall boundary on lines of particles placed along the flume. Reflection in the flume walls has been removed by cropping along the side walls. The particles adjacent to the wall converge both on the swash tip and the wall; particles along the center line only converge on the swash tip. As the wave front propagates, fluid continually moves toward the side walls and remains there due to the no slip condition; the tracking particles are therefore left behind along the wall boundary. Again, sediment and debris in suspension or on the flow surface are likely to behave similarly and converge toward the sides of the channel at the wave front. The influence of the side wall friction on the propagation velocity of the wave front has been considered by Andreini et al. (2012) via the classical concept of hydraulic radius ($R_h$) and a uniform wall shear. For the present experiments, the channel is relatively wide compared to the depth, $d$, so $R_h \approx 0.9d$ instead of $R_h = d$, and the overall influence of the side walls on the momentum balance is therefore also of the order of 10%. To the authors' knowledge, a full analysis of the effect of the convergence of flow toward the side walls does not exist.

Based on the observations over many such tests, a new conceptual model for the flow close to the swash tip is proposed and illustrated in Fig. 12, which shows the relative motion of fluid particles relative to the swash tip. This model ignores the side walls, where a more complex three-dimensional motion occurs at the dual contact line. As the wave tip is approached, the wave front tends toward the vertical, and since the surface is a streamline, propagation of the wave front then requires a rolling motion at the tip. The rolling motion at the tip, somewhat analogous to a caterpillar track, suggests that the front can roll over roughness elements at the bed, as well as flow over or through roughness elements. This suggests that the flow may be less sensitive to increases in bed roughness than would be the case for a steady uniform flow. For example, Baldock and Holmes (2007) observed only small differences in run-up of swash over fixed sediment beds with a factor 3 grain size difference.

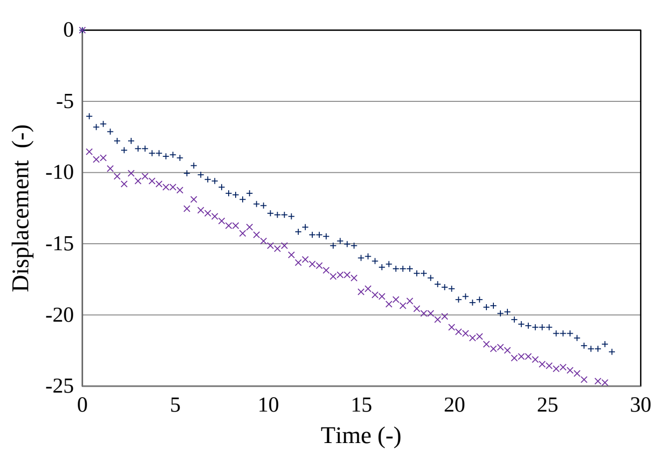


**Fig. 8.** Relative displacement of the swash tip and two particles at the bed. $\alpha = 0.1$, $d_o = 0.11$ m. Detergent 2.

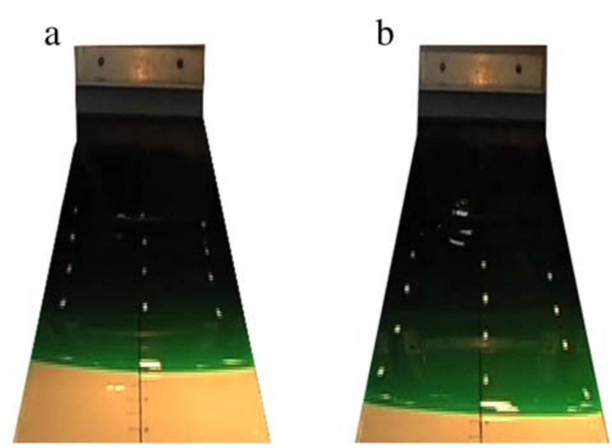


**Fig. 10.** a) Three lines of surface particles shortly after dam release. Initially, the particles in each line are the same distance from the side walls; b) the same particles a few moments later; the leading particles have converged on both the wave front and the side walls. $\alpha = 0.05$, $d_o = 0.12$ m. Detergent 1.

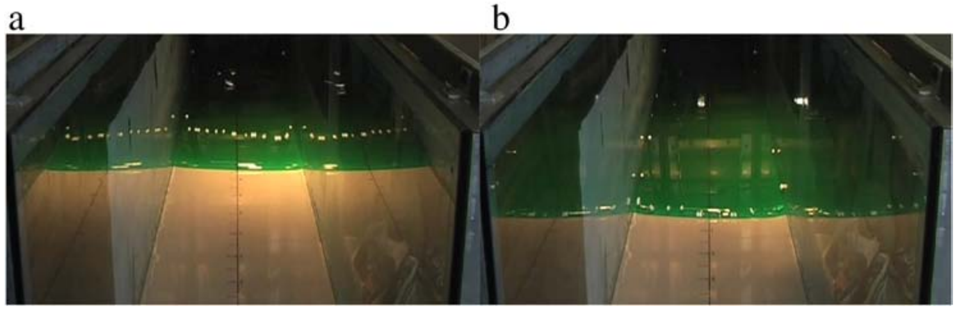


**Fig. 11.** a) A line of surface particles across the flume shortly after dam release; b) the same particles a few moments later. The particles have converged on both the wave front and the side walls; particles are left behind at the wall boundary. $\alpha = 0.05$, $d_o = 0.12$ m. Detergent 1.

## 5. Conclusions

Novel experiments have been performed to track the motion of surface particles close to the wet–dry interface at the bed and walls during viscous swash flows. The experiments clearly show that the no-slip condition at the bed and walls leads to flow convergence at the wet–dry interface at the swash tip. These results are consistent with a simple theoretical model that provides estimates of the rate of this flow convergence. This model is consistent with the earlier work of Huppert (1982) and the boundary layer structure observed by Andreini et al. (2012). The fluid and additional momentum converging on the swash wave tip provides a mechanism to generate the high localized bed shear stresses observed in recent experiments (Barnes and Baldock, 2010). The model and experiments provide useful insights into the likely behavior of suspended sediment and buoyant debris at the leading edge of swash and dam-break flows. This study aimed to demonstrate the convergence effect, rather than provide data for natural swash flows. However, the surface tension is lower in these fluids than for water where turbulent effects should be accounted for by a different boundary layer structure, as outlined in Section 2. Further work is however required to quantify the convergence rate on natural beaches.

Supplementary data to this article can be found online at http://dx.doi.org/10.1016/j.coastaleng.2014.02.008.

## Acknowledgments

Graham Illidge designed the reusable dam gate that seals the reservoir without the need for side-wall fixings that could lead to flow disturbance.

## References

Ancey, C., Cochard, S., Andreini, N., 2009. The dam-break problem for viscous fluids in the high-capillary-number limit. J. Fluid Mech. 624, 1–22.
Ancey, C., Andreini, N., Epely-Chauvin, G., 2012. Viscoplastic dambreak waves: review of simple computational approaches and comparison with experiments. Adv. Water Resour. 48, 79–91.
Andreini, N., Epely-Chauvin, G., Ancey, C., 2012. Internal dynamics of Newtonian and viscoplastic fluid avalanches down a sloping bed. Phys. Fluids 24, 053101.
Baldock, T.E., Holmes, P., 2007. Swash hydrodynamics ona steep beach. Proc. Coastal Dynamics, 97. ASCE, Plymouth, UK.
Baldock, T.E., Grayson, R., Torr, B., Power, H.E., 2010. Flow convergence at the tip of a viscous dam-break wave. Proc. Australian Fluids Mechanics Conference, Dec 2010, Auckland, New Zealand.
Barnes, M.P., Baldock, T.E., 2010. A Lagrangian model for boundary layer growth and bed shear stress in the swash zone. Coast. Eng. 57, 385–396.
Barnes, M.P., O'Donaghue, T., Alsina, J.M., Baldock, T.E., 2009. Direct bed shear stress measurements in bore-driven swash. Coast. Eng. 56, 853–867.
Brocchini, M., Svendsen, I.A., Prasad, R.S., Bellotti, G., 2002. A comparison of two different types of shoreline boundary conditions. Comput. Methods Appl. Mech. Eng. 191 (39–40), 4475–4496.
Chanson, H., 2006. Analytical solutions of laminar and turbulent dam break wave. Proceedings of the International Conference on Fluvial Hydraulics, River Flow 2006, Lisbon, pp. 465–474.
Daugherty, R.L., 1977. Fluid Mechanics with Engineering Applications. McGraw-Hill (564 pp.).
Dussan, E.B., Davis, S.H., 1974. On the motion of a fluid–fluid interface along a solid surface. J. Fluid Mech. 65, 71–95.
Emmett, M., Moodie, T.B., 2008. Dam-break flows with resistance as agents of sediment transport. Phys. Fluids 20 (086603-086603-20).
Goodwin, R., Homsy, G.M., 1991. Viscous flow down a slope in the vicinity of a contact line. Phys. Fluids A3, 515–528.
Griffiths, R.W., 2000. The dynamics of lava flows. Annu. Rev. Fluid Mech. 32, 477–518.
Guard, P.A., Baldock, T.E., 2007. The influence of seaward boundary conditions on swash hydrodynamics. Coast. Eng. 54, 321–331.
Hogg, A.J., Matson, G.P., 2009. Slumps of viscoplastic fluids on slopes. J. Non-Newtonian Fluid Mech. 158, 101–112.
Hogg, A.J., Pritchard, D., 2004. The effects of hydraulic resistance on dam-break and other shallow inertial flows. J. Fluid Mech. 501, 179–212.

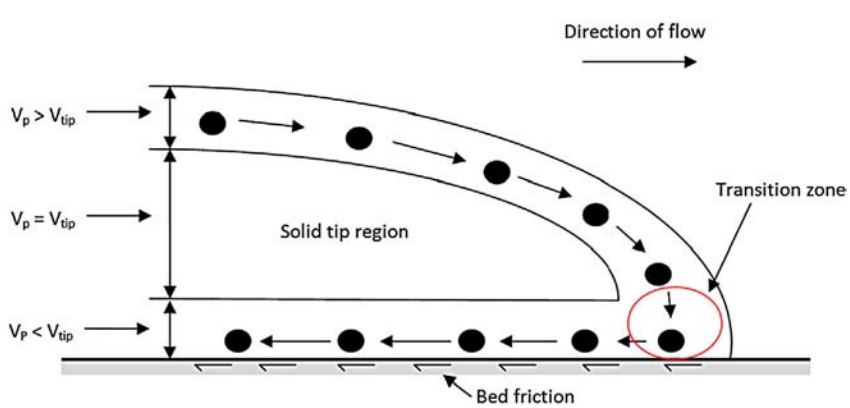


**Fig. 12.** Sketch of proposed new swash tip model. Arrows indicate relative motion of particle with respect to the wave-tip. The transition zone is where particle velocities change from exceeding the wave-tip celerity to becoming slower than the tip celerity. Particles on the bed are assumed to obey a no-slip condition. An internal region behaves as the solid tip model, i.e. where $\overline{u}\approx c$. This region will have a boundary layer structure in reality.

Hughes, M.G., 1995. Friction factors for wave uprush. J. Coast. Res. 11 (4), 1089–1098.
Huppert, H.E., 1982. Flow and instability of a viscous current down a slope. Letters to Nature. Nature 300, 427–429.
O'Donoghue, T., Pokrajac, D., Hondebrink, L.J., 2010. Laboratory and numerical study of dambreak-generated swash on impermeable slopes. Coast. Eng. 57 (5), 513–530.
Othman, I.K., Baldock, T.E., Callaghan, D.P., 2014. Measurement and modelling of the influence of grain size and pressure gradient on swash uprush sediment transport. Coast. Eng. 83, 1–14.
Park, Y.S., Liu, P.L.F., Chan, I.C., 2012. Contact line dynamics and boundary layer flow during reflection of a solitary wave. J. Fluid Mech. 707, 307–330.
Pritchard, D., Guard, P.A., Baldock, T.E., 2008. An analytical model for bore-driven run-up. J. Fluid Mech. 610, 183–193.
Puleo, J.A., Holland, K.T., 2001. Estimating swash zone friction coefficients on a sandy beach. Coast. Eng. 43, 25–40.
Whitham, G.B., 1955. The effects of hydraulic resistance in the dam-break problem. Proc. R. Soc. Lond. A 227, 399–407.
Yeh, H., 2006. Maximum fluid forces in the tsunami runup zone. J. Waterw. Port Coast. Ocean Eng. ASCE 132 (6), 496–500.